Electronic coherences excited by an ultra short pulse are robust with respect to averaging over randomly oriented molecules as shown by singular value decomposition

Manuel Cardosa-Gutierrez[1], R. D. Levine[2,3,4], F. Remacle[1,2*]

[1]Theoretical Physical Chemistry, UR MOLSYS, University of Liege, Belgium
[2]Fritz Haber Center, Institute of Chemistry, The Hebrew University of Jerusalem, Jerusalem 91904, Israel
[3] Department of Molecular and Medical Pharmacology, David Geffen School of Medicine
and
[4] Department of Chemistry and Biochemistry, University of California, Los Angeles, CA 90095, USA

Abstract

We report a methodology for averaging quantum photoexcitation vibronic dynamics over the initial orientations of the molecules with respect to an ultrashort light pulse. We use singular value decomposition of the ensemble density matrix of the excited molecules which allows identifying the few dominant principal molecular orientations with respect to the polarization direction of the electric field. The principal orientations provide insights on the specific stereodynamics of the corresponding principal molecular vibronic states. The massive compaction of the vibronic density matrix of the ensemble of randomly oriented pumped molecules enables a most efficient fully quantum mechanical time propagation scheme. Two examples are discussed for the quantum dynamics of the LiH molecule in the manifolds of its electronically excited Σ and Π states. Our results show that electronic and vibrational coherences between excited states of the same symmetry are resilient to averaging over an ensemble of molecular orientations and can be selectively excited at the ensemble level by tuning the pulse parameters.

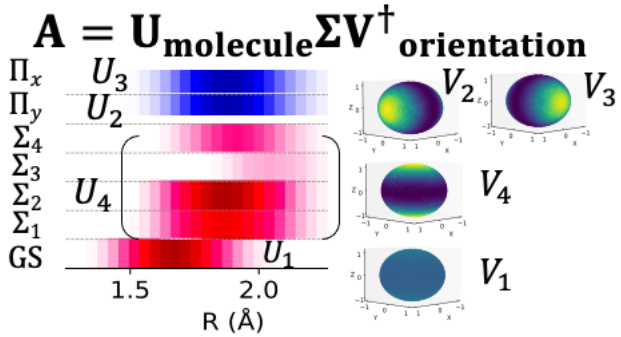

TOC

*Corresponding author: F. Remacle, fremacle@uliege.be

Introduction

Recent progress in attoscience[1-3] open the way to new avenues for controlling chemical reactivity through the selective excitation of a superposition of electronic states with the short-in-time-broad-in-energy attopulse.[4] As pointed out very early,[5] the orientation of the molecule with respect to the polarization direction of the pulse electric field is a very effective way to control the initial superposition built by the pulse and therefore the subsequent dynamics. Molecules can be aligned or oriented using a single or a sequence of laser pulses, enabling to carry out field free photoexcitation or photoionization experiments in the molecular frame. [6-10] However, the achievable orientation is typically limited to values of $\langle \cos\theta \rangle \approx 0.7$ and $\langle \cos^2\theta \rangle \approx 0.8$. Moreover, the proposed experimental approaches to align or orient molecules are not applicable to all types of molecules.[11-13] Therefore, it is often the case that a realistic description of quantum dynamics of molecules photoexcited by short atto and few fs pulses requires an averaging over the molecular orientations with respect to the polarization direction of the exciting optical pulse. However, averaging quantum dynamics simulations over an ensemble of molecular orientations can be computationally rather costly in computer time and storage capacity since the quantum dynamical propagation needs to be repeated as many times as the number of molecular orientations in the ensemble. This is particularly so when the pulse parameters other that the polarization direction need to tuned to control the vibronic dynamics which requires to repeat the ensemble averaging needs a large number of times. While orientation averaging is manageable computationally for the vibronic quantum dynamics of diatomic molecules in a superposition of several electronic states, it becomes out of reach for quantum dynamical simulation involving several nuclear degrees of freedom on coupled electronic states, as typical when molecules and molecular cations are excited by ultrashort, broad in energy atto pulses.[2, 14-18] Even for a diatomic molecule, tuning the pulse parameters for an ensemble of molecular orientations becomes computationally very demanding in memory capacity and computer time.

Here we propose a numerical approach for computing the ensemble dynamics of randomly oriented molecules interacting with an ultrashort optical pulse that considerably lowers the cost in computational resources and provides insights on the orientation effects. Our approach is based on the Singular Value Decomposition (SVD)[19] of the matrix built from the pure quantum states associated with each molecular orientation of the ensemble. This matrix, **A**, is a rectangular matrix with dimension, N_b, the number of vibronic basis functions used to expand the wave function, times the number of molecular orientations, N_o. Typically, when the pulse

is over, only a few principal components suffice to obtain an accurate description of the matrix **A**. The SVD principal components identify the most important orientations that contribute to the ensemble dynamics (the singular orientation vectors) and the corresponding oriented molecular pure quantum states (the singular molecular states). Each of these molecular pure quantum states evolves in time in a specific way that it is dictated by the principal orientation to which it corresponds. One therefore gets insights on the dynamics in specific orientations whose relative weight in the ensemble can be tuned by the pulse parameters other than its polarization direction: the duration and the carrier frequency of the pulse. Valuable stereo dynamics insights are therefore gained for ensemble of randomly oriented molecules.

In addition we show that the SVD compaction significantly reduces the cost of computing the quantum dynamics of the ensemble since only few singular (pure) oriented molecular quantum states need to be stored and propagated after the pulse to accurately describe the ensemble quantum dynamics. An exact description is obtained by retaining as the number of principal components the smallest dimension of **A** matrix, which is typically the number of orientations, N_o. For an approximate description, one can adjust the number of retained principal components necessary to reach a specified accuracy threshold. We find that only a few components are required for a satisfactory semi-quantitative description.

Methods : SVD approach to coupled electrons-nuclei quantum dynamics averaged over random molecular orientations

At time $t = 0$, the molecules of the ensemble are in their ground electronic state. The different molecules of the ensemble are distributed over their particular orientation, o, with respect to the polarization direction of the exciting pulse. Each initial orientation, o, at the time before excitation defines a pure state, $\left|\Psi_o\left(t=0\right)\right\rangle$. During and after the excitation by the atto pulse each initial state evolves into $\left|\Psi_o\left(t\right)\right\rangle$, a coherent combination represented as a Born-Huang expansion, a sum of N_b separable terms in the nuclear and electronic degrees of freedom:

$$\left|\Psi_o\left(t\right)\right\rangle = \sum_{b=1}^{Nb} c_b^o\left(t\right)\left|b\right\rangle \qquad (1)$$

where $c_b^o\left(t\right)$ is the Born-Huang amplitude of the vibronic basis function $\left|b\right\rangle$ for the initial orientation, o. The index b stands for a nuclear and an electronic index which, for a pulse broad in energy, includes several coupled electronic states. In general we expect that the number of terms in Eq. (1) is such that $N_b >> N_o$, where N_o is the number of molecular

orientations in the ensemble. The amplitudes $c_b^o(t)$ are computed by integrating the Time-Dependent Schrödinger Equation (TDSE), for a basis of N_g grid functions, $|g\rangle$, for the nuclear coordinates and N_e coupled adiabatic electronic states, $|i\rangle : |b\rangle = |g\rangle|i\rangle$, which leads to a total dimension $N_b = N_g$ x N_e for the vector of the amplitudes $\mathbf{c}_o$:

$$i\hbar \frac{d\mathbf{c}_o}{dt} = \mathbf{H}\mathbf{c}_o \qquad (2)$$

The inequality $N_b >> N_o$ is primarily because the number N_g of grid points needs to be large. The molecular Hamiltonian, **H**, includes the coupling to the electric field of the pulse, $\mathbf{E}(t)$, in the dipole approximation and the non adiabatic coupling (NAC) between the electronic states driven by the nuclear motion. For a non rotating diatomic molecule,

$$\mathbf{H} = -\frac{1}{2\mu}\left(\nabla_R^2 + 2\boldsymbol{\tau}(R).\nabla_R + \left(\nabla_R \boldsymbol{\tau}(R)\right) + \boldsymbol{\tau}(R).\boldsymbol{\tau}(R)\right) + \mathbf{V}(R) - \mathbf{E}(t).\boldsymbol{\mu} \qquad (3)$$

In Eq. (3), the τ is the non adiabatic coupling between electronic states, $\tau_{ij}(R) = \langle \phi_i^{ele} | \nabla_R | \phi_j^{ele} \rangle$ and **V**(*R*) the potential term. The last term is the dipole coupling where μ is the total dipole operator, $\mu = \mu^{nuc} + \mu^{ele}$. The electric field is given by

$$\mathbf{E}(t) = \frac{d\mathbf{A}(t)}{dt} = \hat{\mathbf{e}}|E_0| \exp\left(-\frac{(t-t_p)^2}{2\sigma_p{}^2}\right)\left(\cos\left(\omega_p(t-t_p)\right) - \left(\frac{t-t_p}{\omega_p \sigma_p^2}\right)\sin\left(\omega_p(t-t_p)\right)\right) \qquad (4)$$

In Eq. (4), $|E_0|$ is the strength of the pulse. The pulse is confined in a Gaussian envelope centered at t_p, with a carrier frequency ω_p and a Full Width at Half Maximum (FWHM) given by $2\sqrt{2\ln 2}\,\sigma_p$. The orientation of the electric field vector, $\hat{\mathbf{e}}$, is defined in the molecular frame attached to the center of mass of the molecule. This considerably simplifies the numerical integration and is equivalent to defining the orientation of the molecular frame with respect to the orientation of the electric field in the laboratory frame. Note that one needs to rotate back to the laboratory frame before analyzing angular distributions.

During the pulse, the Hamiltonian depends on time and each polarization direction of the pulse defines a specific dynamics. For an ensemble of molecular orientations, one therefore needs to average the dynamics over the ensemble. We do so by integrating the TDSE during the pulse

for an ensemble of N_o orientations of $\mathbf{E}(t)$, each computed separately, obtaining N_o time-dependent pure states $\left|\Psi_o(t)\right\rangle$. These states are gathered into a rectangular, complex, N_b x N_o, matrix **A** with typically $N_o < N_b$. Singular Value Decomposition (SVD) provides an exact description of the matrix **A** as a sum of a maximum of N_o separable terms, its principal components.[19] The SVD factorization of **A** is a sum of direct products of a left, $\mathbf{U}_m$, and a right, $\mathbf{V}_m^\dagger$, singular complex eigenvector weighted by the corresponding (real) singular value, σ_m,

$$\mathbf{A}(t) = \sum_{m=1}^{N_o} \sigma_m(t)\ \mathbf{U}_m(t) \otimes \mathbf{V}_m^\dagger(t) \qquad (5)$$

In each principal component, m, the right singular vector, $\mathbf{V}_m(t)$, has N_o components, $v_{om}(t)$, and depends only on the orientation index, o, and the left singular vector, $\mathbf{U}_m(t)$, has N_b components, u_{bm}, and depends only on the basis set index b. Throughout, we refer to $\mathbf{V}_m(t)$ as the orientation singular vector and to $\mathbf{U}_m(t)$ as the molecular singular vector.

From the rectangular **A** matrix, one can construct two reduced square density matrices. The N_b x N_b density matrix of the ensemble of molecules, $\rho_{mol}(t)$, is the trace over the orientations and depends on the molecular degrees of freedom only. It is the $\mathbf{AA}^\dagger$ quadratic form of the matrix $\mathbf{A}(t)$: [20],

$$\rho^{mol}(t) = (1/N_o)\mathbf{A}\mathbf{A}^\dagger = (1/N_o)\sum_{o=1}^{N_o} \mathbf{c}_o(t)\mathbf{c}_o^\dagger(t) = (1/N_o)\sum_{b=1}^{N_b}\sum_{b'=1}^{N_b} |b\rangle\left(\sum_{o=1}^{N_o} c_b^o(t)c_{b'}^o{}^*(t)\right)\langle b'| \qquad (6)$$

The matrix elements of $\rho^{mol}(t)$ are the average populations and coherences between the basis set functions $|b\rangle = |g\rangle|i\rangle$. $\rho^{mol}(t)$ is a function of the molecular singular vectors only. Inserting Eq. (5) into Eq. (6), one gets

$$\begin{aligned}
\rho^{mol}(t) &= (1/N_o)\sum_{m,m'} \sigma_m(t)\sigma_{m'}(t)\left(\mathbf{U}_m \otimes \mathbf{V}_m^\dagger\right).\left(\mathbf{V}_{m'} \otimes \mathbf{U}_{m'}^\dagger\right) \\
&= (1/N_o)\sum_{m,m'} \sigma_m(t)\sigma_{m'}(t)\left(\mathbf{U}_m \otimes \left(\mathbf{V}_m^\dagger.\mathbf{V}_{m'}\right) \otimes \mathbf{U}_{m'}^\dagger\right) \qquad (7) \\
&= (1/N_o)\sum_{m} \sigma_m^2(t)\left(\mathbf{U}_m \otimes \mathbf{U}_m^\dagger\right) = (1/N_o)\sum_{m} \sigma_m^2(t)\rho_m^{mol}(t)
\end{aligned}$$

where the last line results from the orthogonality of the orientation singular vectors: $\mathbf{V}_m^\dagger\mathbf{V}_{m'} = \delta_{mm'}$. Each singular vector leads to a principal molecular density matrix, $\rho_m^{mol}(t)$,

which in turn defines a reduced nuclear and a reduced electronic density matrix, thereby providing insights of the vibrational and electronic coherences of the principal orientations.

$$\rho_{nuc}^{mol}(t)=\mathrm{Tr}_{ele}\left(\rho^{mol}(t)\right)=\left(1/N_o\right)\sum_{m}^{Nmin}\sigma_m^2\mathrm{Tr}_{ele}\left(\rho_m^{mol}(t)\right)=\left(1/N_o\right)\sum_{m}^{Nmin}\sigma_m^2\rho_{nuc,m}^{mol}(t) \quad (8)$$

whose off diagonal elements correspond to the coherences between points of the nuclear grid and its diagonal elements to the average localization of the vibronic wave packet on the grid. Tracing $\rho^{mol}(t)$ over grid points provides the reduced electronic density matrix:

$$\rho_{ele}^{mol}(t)=\mathrm{Tr}_{g}\left(\rho^{mol}(t)\right)=\left(1/N_0\right)\sum_{m=1}^{Nmin}\sigma_m^2\mathrm{Tr}_{g}\left(\rho_m^{mol}(t)\right)=\left(1/N_0\right)\sum_{m=1}^{Nmin}\sigma_m^2\rho_{ele,m}^{mol}(t) \quad (9)$$

Similarly, one can define the complementary N_o x N_o reduced orientation density matrix, $\rho^{orien}(t)$, by the quadratic form $\mathbf{A}^{\dagger}\mathbf{A}$:

$$\rho^{orien}(t)=\left(1/N_0\right)\mathbf{A}^{\dagger}\mathbf{A} \quad (10)$$

with matrix elements given by

$$\boldsymbol{\rho}_{oo'}^{orient}(t)=\left(\frac{1}{N_o}\right)\sum_{b=1}^{N_b}c_b^{o}*(t)c_b^{o'}(t)=\begin{cases}\left(1/N_0\right)\text{ if } o\equiv o'\\ <\left(1/N_0\right)\text{ otherwise}\end{cases} \quad (11)$$

$\rho^{orien}(t)$ depends on the orientation singular vectors only. Using Eq. (5)

$$\begin{aligned}\rho^{orien}(t)&=\left(1/N_o\right)\sum_{m,m'}\sigma_m(t)\sigma_{m'}(t)\left(\mathbf{V}_m\otimes\mathbf{U}_m^{\dagger}\right).\left(\mathbf{U}_{m'}\otimes\mathbf{V}_{m'}^{\dagger}\right)\\&=\left(1/N_o\right)\sum_{m,m'}\sigma_m(t)\sigma_{m'}(t)\left(\mathbf{V}_m\otimes\left(\mathbf{U}_m^{\dagger}.\mathbf{U}_{m'}\right)\otimes\mathbf{V}_{m'}^{\dagger}\right)\\&=\left(1/N_o\right)\sum_{m}\sigma_m^2(t)\left(\mathbf{V}_m\otimes\mathbf{V}_m^{\dagger}\right)=\left(1/N_o\right)\sum_{m}\sigma_m^2(t)\rho_m^{orien}(t)\end{aligned} \quad (12)$$

Note that the two partial traces, $\rho^{mol}(t)$ and $\rho^{orien}(t)$, have the same set of eigenvalues, which are the square of the singular values, σ_m, of the matrix **A**:

$$\mathrm{Tr}\left[\rho_{mol}(t)\right]=\mathrm{Tr}\left[\rho_{orien}(t)\right]=\left(\frac{1}{N_o}\right)\sum_{m=1}^{N_o}\sigma_m^2(t)=1. \quad (13)$$

with $\sum_{m-1}^{N_o}\sigma_m^2(t)=N_o$.

We define a set of 800 orientations on the unit sphere. Each orientation is a 3 dimensional vector in the molecular frame: $\hat{e}_o=x_o\hat{e}_x+y_o\hat{e}_y+z_o\hat{e}_z$. The orientation density matrix before interacting with the molecule is defined by the scalar products between all the vectors $\hat{e}_0$.

Gathering the vectors $\hat{e}_0$ in a N_o x 3 matrix **e** in which each row is given by the Cartesian components (x_0, y_0, z_0) of a vector $\hat{e}_0$, we can write $\rho^{orien}(0) = \mathbf{e}\mathbf{e}^T$. Initially there are at most three principal orientation vectors, one along x, one along y and one along z. Note that the N_o x N_o matrix $\rho^{orien}(0)$ is off diagonal. The off diagonal elements will be large when the two orientations oo' are close to one another.

In the sudden approximation for the photoexcitation, i.e. a one photon transition at time t_p when the pulse is maximum, Eq. (4), and restricting the dynamics to the excited states, the initial amplitudes at each point of the nuclear grid in each excited electronic state can be factorized as the scalar product of the orientation of the electric field, $\hat{\mathbf{e}}_0$, and the transition dipole moment from the ground electronic state $\boldsymbol{\mu}_{GS-gi}^T = \left(\mu_{GS-gi}^x, \mu_{GS-gi}^y, \mu_{GS-gi}^z\right)$:

$$c_{gi}^0 = \hat{\mathbf{e}}_0^T . \boldsymbol{\mu}_{gi} \tag{14}$$

We show in the SI that then $\rho^{mol}(t_p)$ is given by

$$\rho^{mol}(t_p) = \boldsymbol{\mu}\boldsymbol{\mu}^T \tag{15}$$

where $\boldsymbol{\mu}$ is ((Ne-1)xNg) x 3 matrix of the cartesian components of transition dipole between the GS and the excited states at each grid point. $\rho^{mol}(t_p)$ is independent of the polarization direction of the electric field of the pulse for an ensemble of randomly oriented molecules. It can only have 3 principal components oriented along the three cartesian axis of the molecular frame. We have previously used this result for describing the ultrafast vibronic Jahn-Teller structural rearrangement induced by the sudden photoionization of methane[21] using a 3 electronic state 2 nuclear degrees of freedom model.

Here we go beyond the sudden approximation limit and treat the case of stronger pulses entangle the orientations and the intramolecular nuclear and electronic degrees of freedom and induce transient vibronic dynamics. The non linear excitation process leads to a time dependence of the singular values $\sigma_m(t)$ and of the molecular and orientation singular vectors in Eq. (5). When the pulse is over, the dipole coupling terms vanish and the Hamiltonian, Eq. (3), becomes stationary. Then the singular values become stationary since we consider a non rotating molecule.

The SVD of the **A** matrix at the end of the pulse, at time t_i, therefore provides a set of orthogonal pure states, $\mathbf{U}_m$, that each corresponds to a specific singular orientation of the molecule as

defined by the corresponding orientation singular vector $\mathbf{V}_m$. We show below that only a few singular values, $\sigma_m(t_i)$, $3 < N_{\min} \le N_o$, suffice to recover accurately the molecular density matrix averaged over the molecular orientations, $\rho^{mol}(t_i)$, at the end of the pulse, t_i (Eq. (7)). The minimum number of principal components is larger than 3 because of the transient dynamics occuring during the pulse which entangles the nuclear and electronic molecular degrees of freedom with the orientation of the pulse electric field and the fact that the dynamics in the GS is included. One can set the maximum number of singular values, $\sigma_m(t_i)$, needed to describe the dynamics by putting a threshold on how well the norm of $\rho^{mol}(t_i)$ is recovered:

$$\Delta_{Nmin} = 1 - \mathrm{Tr}\left[\rho^{mol}_{Nmin}(t_i)\right] = 1 - \left(\frac{1}{N_o}\right)\sum_{m=1}^{Nmin} \sigma_m^2(t_i) \ge 0 \qquad (16)$$

Since the singular values are stationary, one can set up a very efficient propagation scheme for the density matrix of the ensemble of molecules, $\rho^{mol}(t)$, after the pulse, by propagating with the molecular Hamiltonian (Eq. (3)) only the few, $Nmin$, $\mathbf{U}_m$ vectors that correspond to the largest singular values:

$$i\hbar\, d\mathbf{U}_m/dt = \mathbf{H}\mathbf{U}_m \text{ for } t > t_i, \text{ with } \mathbf{U}_m(t_i) = \sum_{b=1}^{Nb} u_{bm}(t_i)\left|b\right\rangle \qquad (17)$$

where the initial values, $u_{bm}(t_i)$, are the coefficients of the $\mathbf{U}_m$ vectors at the time t_i (the end of the pulse).

Providing that the TDSE is integrated accurately so that the integration error is smaller that Δ_{Nmin}, the numerical error, Eq. (16), that is due to the fact that we use a restricted number of principal components of the matrix **A,** does not increase with time. Using Eq. (7), we get

$$\begin{aligned}\rho^{mol}_{Nmin}(t) &= (1/N_o)\sum_{m=1}^{N_{min}} \sigma_m^2(t_i) \sum_{b}^{Nb} \sum_{b'}^{Nb'} u^*_{bm}(t) u^*_{b'm}(t) \left|b\right\rangle\left\langle b'\right| \\ &= (1/N_o)\sum_{m=1}^{Nmin} \sigma_m^2(t_i)\, \rho^{mol}_m(t)\end{aligned} \qquad t > t_i \qquad (18)$$

To summarize, our approach requires to propagate all the initial states defined by a sampling of the molecular orientations until the pulse is over. Since we consider excitation by short atto or few, 1-2, fs pulses, this propagation time is short, of the order of 20 fs for a pulse with a FWHM of 2 fs. Then when the Hamiltonian is stationary, one performs an SVD analysis of the matrix **A** (Eq. (5)) and retains the $N_{\min}$ largest principal components necessary to reach a specified accuracy threshold. Only these fewer components need to be propagated after the

pulse using the TDSE as long as the molecular Hamiltonian remains stationary. This approach reduces the computer time needed to compute quantum molecular dynamics averaged over molecular orientations by at least 2 orders of magnitude for the dynamics of a diatomic molecule taking place on several electronic states. The gain is even larger when molecule has several nuclear degrees of freedom. It is also storage efficient because it allows compacting the information of dynamics of the randomly oriented initial states into a few singular components. Using our approach, one does not need to store and analyze the dynamics of all the randomly orientated initial states. Each of the principal molecular vector provides the vibronic stereodynamics corresponding to a specific principal molecular orientation of the ensemble.

Results and discussion

SVD approach to the dynamics of randomly oriented LiH molecules

We apply our scheme to the non rotating LiH molecule excited by two deep UV few cycles pulses of different carrier frequency and with the same FWHM of 2 fs (FWHM bandwidth in energy of 1. 82 eV), Eq. (4). Such pulses are ideally suited to excite neutral polyatomic molecules by one photon excitation and their generation has recently been reported. [22-24] LiH has a rotational period of 4.4 ps which justifies the fact that there is no coupling to rotations during the pulse and for the next 200 fs of the dynamics. In the Franck-Condon (FC) region, R_{eq} = 1.6Å (see Figure S2a), the transition dipole moment from the GS to the lowest Σ state, Σ_1, along z is smaller than the transition dipole along x or y to the lowest Π state, Π_1, and to the higher Σ and Π states. We report on the dynamics induced using pulses with two different carrier frequencies, ω_p, tuned to access different combinations of Σ and Π states. The first pulse has a carrier frequency of 4.35 eV, so that both the lowest Σ_1 and Π_1 states fall within the pulse energy bandwidth. However, because of the difference in the transition dipole moments, for random orientations, it is the Π_1 state that is accessed, with only very low populations in Π_3, in Σ_1 and in the entire Σ manifold. The second pulse has a higher carrier frequency of 5.17 eV which allows accessing the higher Σ and Π states with similar probabilities. The strength of the electric field, $|E_0|$ is 0.01 a.u. (3.51 10^{12} W/cm^2) for both pulses. A field strength of ≈10^{12} W/cm^2 is at the higher end of the range of currently available 1-2 fs DUV pulses.[22-24] It is also low enough to avoid photoionization by two photon absorption. As discussed below, this field strength is large enough to induce non linear effects

and transient population dynamics during the excitation process and entangle the orientations with the intramolecular degrees of freedom.

The dynamics induced by the first pulse is used for benchmarking the SVD approach for random initial molecular orientations. Excitation by the 4.35 eV pulse yields very different populations: the population of the Π_1 state is 1-2 orders of magnitude larger than that of the Σ and the Π_3 states. To benchmark our approach, we computed the time evolution by solving the TDSE for 800 random initial orientations using Eq. (2) for 200 fs. The electronic structure parameters (potential energy, transition dipole and NAC curves) are those reported in ref. [25] and plotted in the SI (figures S1, S2a-d and S3a-c). The NAC terms couple electronic states of the same symmetry, Σ or Π. Electric fields oriented along the molecular axis (the *z* axis in the molecular frame (see inset of Figure S1) can only access excited Σ states since the ground state is of Σ symmetry. However, as soon as the electric field has components along x or y in the molecular frame, a linear combination of Σ and Π states is excited. Since the transition dipole to the Π_1 state is larger than to the Σ states and to the other Π states, the averaged populations in its two components are much larger than that of the other states. The populations in the electronic states averaged over 800 random molecular orientations are plotted in figure 1a for the Π_1 state and in figure 1b for the Σ manifold and the Π_3 state.

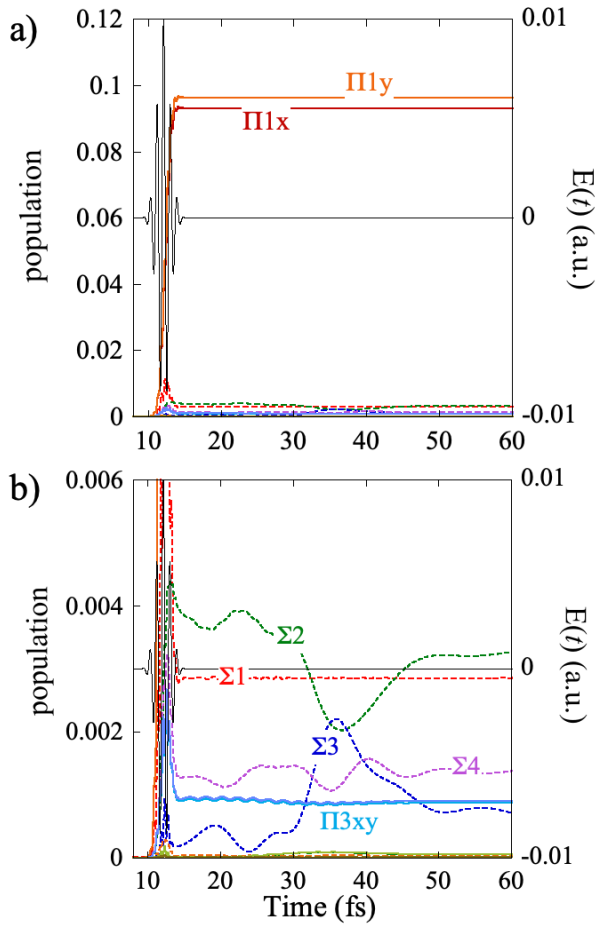

Figure 1. Populations averaged over 800 molecular orientations in the Π_1 state (a) and (b) in the Σ manifold (Σ_2, Σ_3 and Σ_4) and the Π_3 state computed for an excitation by the deep UV 2fs pulse of 4.35 eV. The reason why the two components of the Π_1 state are not exactly equal is due to the fact that only 800 orientations are included in the averaging procedure. After the pulse, the population of the Π_1 state is essentially stationnary. The long time behavior is given in Figure S4.

The electronic states within each manifold are coupled by the NAC terms. As can be seen from Fig 1b, the population transfers are far larger within the states of the Σ manifold than for the Π ones. This is mainly due to the fact that the energy difference between the two lowest Π states is much larger. For the same reason, the population transfers between the Σ_1 state and the higher Σ states are also small.

Our SVD approach to the ensemble dynamics begins by building the matrix **A** (Eq. (5)) from the 800 randomly oriented $\mathbf{c_0}$ vectors and compute its principal components by SVD at every time step during the excitation by the pulse. The singular values are arranged in order of

decreasing magnitude with σ_1 being the largest. The square of the 8 largest singular values, σ_m^2 normalized by N_o, the number of initial random orientations, are plotted in Fig. 2a as a function of time on a log scale to emphasize how fast they decrease in magnitude with increasing order *m*. As discussed above, after the pulse, the Hamiltonian is stationary and the singular values are constant in time. The normalized singular value σ_1 is unity before excitation and remains close to one after the pulse. It can be correlated with the ground electronic state as we discuss below (Figure 4). σ_2 and σ_3 are degenerate during and after the pulse, while σ_6 and σ_7 that are degenerate during the pulse but after the pulse, it is the pair σ_7, σ_8 that are equal. As shown in figure 4 below, these two pairs of singular values are localized on the two Π states, Π_1 and Π_3. One can also see in Figure 2a that a larger number of singular values are important during the pulse than after the pulse, which is due to the entanglement between the orientations and the molecular degrees of freedom during the pulse. The populations of the higher Σ states that are involved in the transient dynamics during the pulse are going back to zero when it is over. Figure 2b shows how much of the trace of the density matrix, $\mathrm{Tr}\left[\rho_{Nmin}^{mol}(t)\right]$ (Eq.(16)) is recovered for an increasing number of singular values, σ_m, *m*= 1 to 5. Five singular values suffice to recover the trace of the density matrix of the ensemble of 800 randomly oriented molecules with a precision better than of 10^{-3} during the pulse and of 10^{-5} after it is over, see Figure 3a. In figure 3b, we plot on a log scale the set of the 25 largest singular values at the maximum of the pulse (12.3 fs) and after the pulse, when the Hamiltonian and therefore the singular values are stationary (18 fs). One can see that indeed the entanglement between orientation and intramolecular degrees of freedom is larger during the transient dynamics induced by the pulse, a 6th singular value would be needed to get an accuracy of 10^{-5} during the pulse. Figure 3b also shows that with 15 eigenvalues, the SVD fit reaches error values of $\approx 10^{-13}$ (numerically zero) which corresponds to the accuracy of the numerical integration of the TDSE.

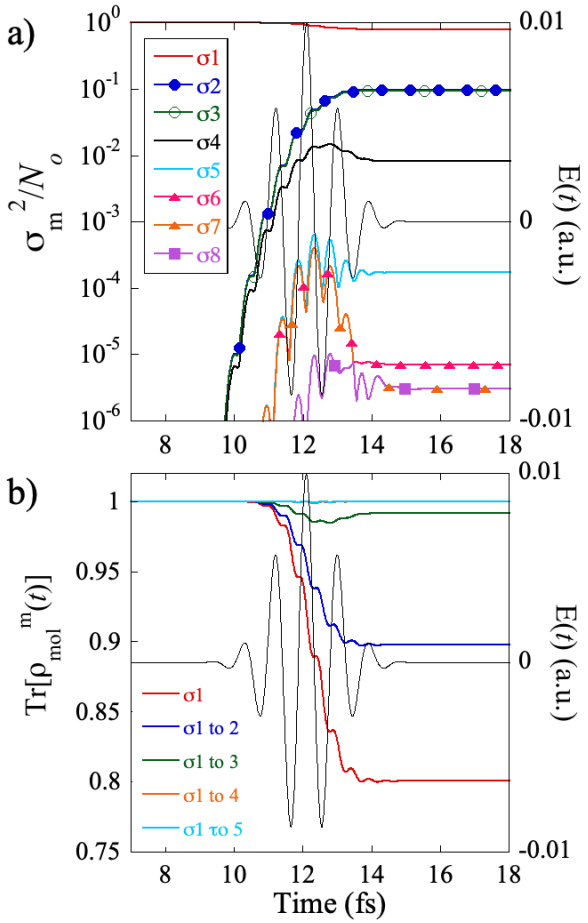

Figure 2. a) The time evolution of the 8 largest normalized singular values, σ_m^2 / N_0, during and after the pulse. The singular values of that correspond to molecular singular vectors $\mathbf{U_m}$ localized on the two components of Π states are plotted with markers so as to better identify them. The two pairs of degenerate singular values localize on the Π states, σ_2 and σ_3 on Π_1 (blue diamonds for Π_{1x} and green ones for Π_{1y}) and σ_6 (red triangles) and σ_7 (orange filled triangles) during the pulse and σ_7 and σ_8 (filled squares) after the pulse on Π_3. b) the cumulative trace recovered with an increasing number of singular values, from 1 to 5.

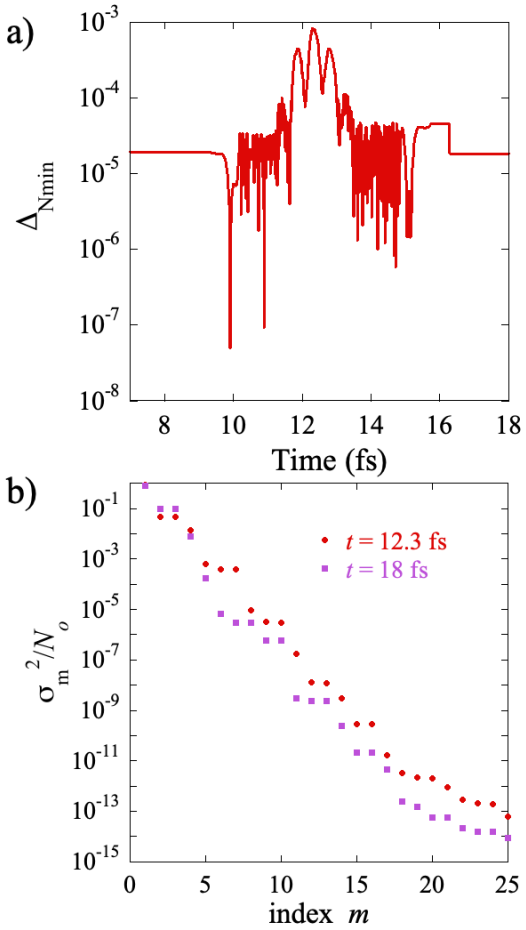

Figure 3: a) $\Delta_{N\min}$ (Eq. (16)) the absolute value on the error on the trace computed by including 5 singular values in the trace of the density matrix, $\mathrm{Tr}\left[\rho^{mol}_{N\min=5}(t)\right]$. b) the 25 largest normalized singular values computed at the maximum of the pulse (violet squares) and after the pulse, when their values are constant (red dots) at 18 fs. The doublets of degenerate singular values correlate with the two components of the Π states.

In figure 4, we show the localization of the molecular (left) singular vectors, $\mathbf{U_m}$, on the electronic states and along the *R* coordinate, at 18fs, after the pulse is over. $\mathbf{U_1}$, which corresponds to the largest singular value, is localized on the ground electronic state and corresponds to the ground vibrational state (the initial state). $\mathbf{U_2}$ and $\mathbf{U_3}$ are localized on the Π_1 state (on the y and x components respectively) with essentially equal values of σ_2 and σ_3. $\mathbf{U_4}$ is localized on the manifold of excited Σ states ($\Sigma_1, \Sigma_2, \Sigma_3, \Sigma_4$) with a σ_4 value an order of magnitude smaller than σ_2 and σ_3. $\mathbf{U_5}$ is localized on the GS but corresponds to excited vibrational states, with an even smaller value of σ_5.

The corresponding singular orientation vectors are shown in figure 5a-d. $\mathbf{V_1}$ (panel a) is distributed uniformly on the sphere, corresponding to the initial distribution of orientations, in agreement with the localization of $\mathbf{U_1}$ on v =0 of the ground electronic state (see Figure 4). $\mathbf{V_2}$ (panel c) and $\mathbf{V_3}$ (panel d) are localized along the y and the x axis respectively since $\mathbf{U_2}$ and $\mathbf{U_3}$ are localized in the y and x components of the Π_1 state. $\mathbf{V_4}$ (panel b) is localized along the z axis since it corresponds to excited Σ states. $\mathbf{V_5}$ (figure S5) is a much smaller component and corresponds to excited vibrational state of the GS and is localized on z. We therefore see that the localization of the singular vectors is dictated by the symmetry the electronic states, which is conserved after the pulse since the NAC terms can only couple states of the same symmetry. The carrier frequency of the pulse induces one photon transitions, which means that during the pulse, the GS of Σ symmetry is coupled to the Π states, which breaks the Σ - Π symmetry, and couples in second order the Π states with the excited Σ states. This explains the higher degree of entanglement between orientations and the intramolecular degrees of freedom during the pulse discussed above. The effect here remains limited because the excited Σ and Π are populated by one photon transitions and the pulse remains relatively weak.

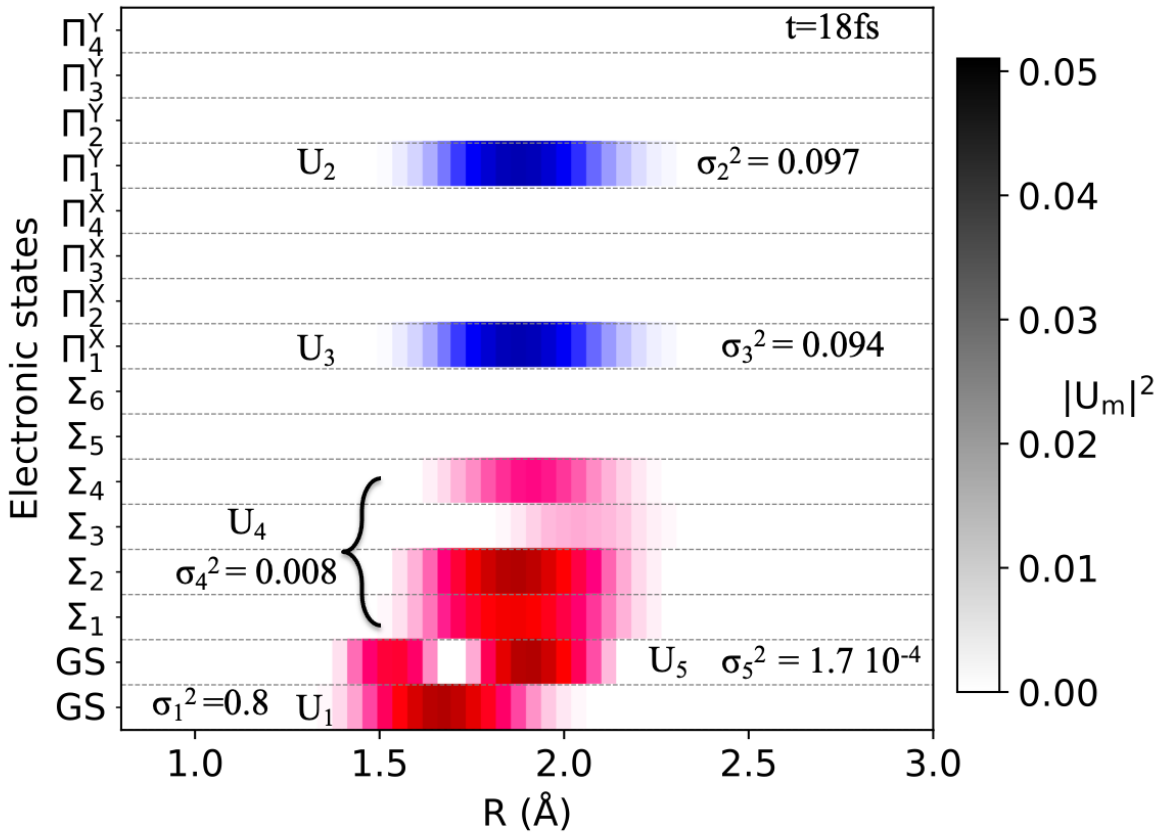

Figure 4: Localization of the molecular singular vectors $\mathbf{U_m}$ on the grid for the 5 largest singular values. Computed for the excitation by the 2fs 4.35 eV pulse.

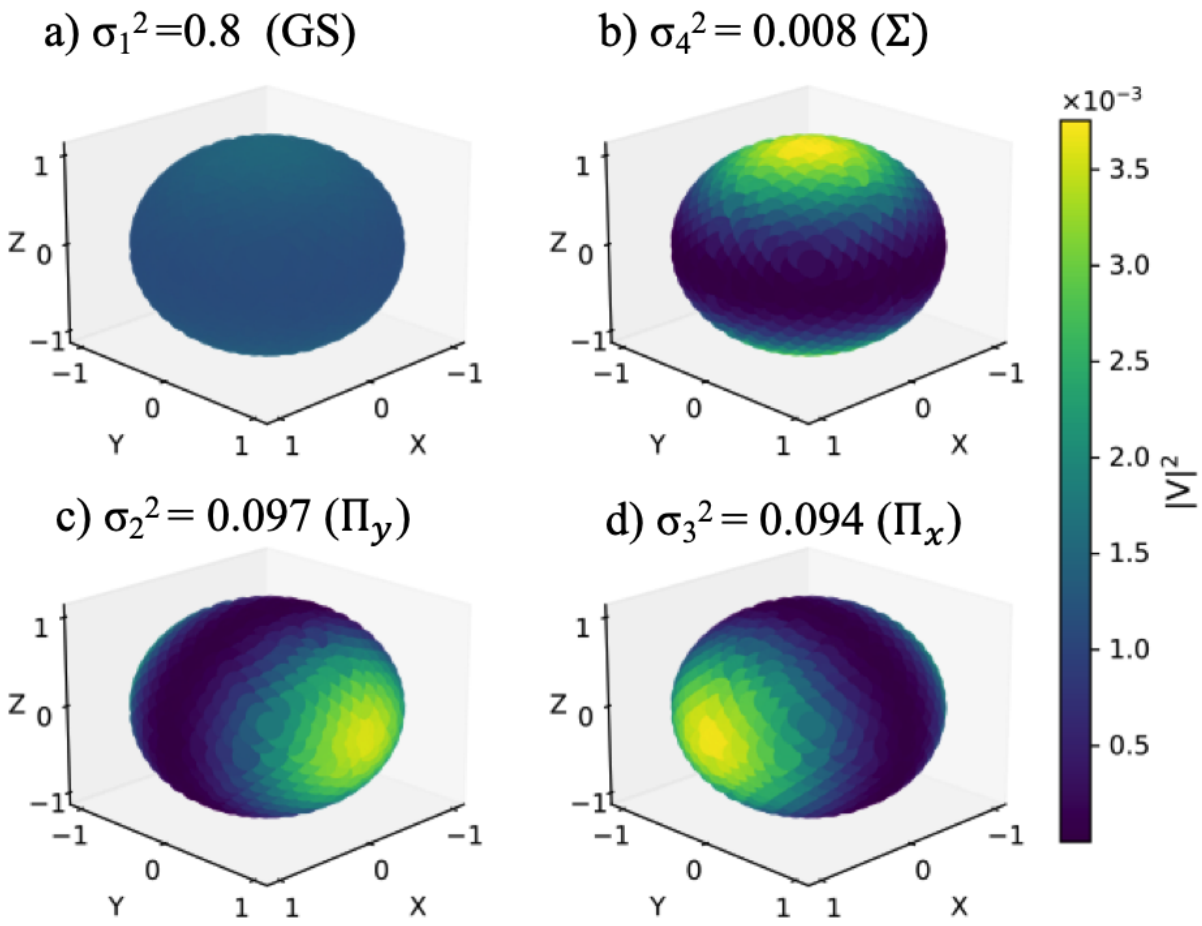

Figure 5: Orientation distribution on the unit sphere of the square modulus of the **V** vectors of the 4 largest principal components. $\mathbf{V_1}$ (a)is uniformly distributed over all orientations. $\mathbf{V_2}$ (c) and $\mathbf{V_3}$ (d) are oriented along y and x respectively to account for the excitation of the Π states while $\mathbf{V_4}$ (b) is oriented along z and accounts for the excitation of the Σ excited states. The colors code on the rhs is common to $\mathbf{V_2}$, $\mathbf{V_3}$ and $\mathbf{V_4}$. The V vectors are normalized to 1. $\mathbf{V_5}$, that is oriented along z as well, which corresponds to a more minor principal component. It shown in Figure S5.

Since the Hamiltonian is stationary after the pulse, the left eigenvectors, $\mathbf{U_m}$, which are localized on the grid and on the electronic states, can be used to compute the quantum dynamics of the ensemble. We do so using Eq. (10) by propagating numerically the 5 $\mathbf{U_m}$ vectors that correspond to the five largest singular values, σ_m, starting at the end of the pulse, t_i =18 fs. Since the numerical precision of the integration is of the order of 10^{-12} for the 200 fs of the propagation time, the error that we make by retaining the 5 largest principal components (10^{-5} relative error on the trace of the density matrix $\rho^{mol}(t)$) does not increase. In parallel, as a

benchmark, we propagated the 800 initial states separately for 200 fs using the TDSE and the performed the averaging over these 800 $\left|\Psi_o(t)\right\rangle$.

The agreement between the 'exact' and the 'SVD' ensemble averaging computations is excellent for the populations of electronic states, electronic coherences and for observables such as the time-dependent dipole moment, which depends on both the populations and the coherences between electronic states and grid points. This is true not only for the states with a large population, like the two components of the Π_1 state and the GS plotted in Figure 1a, but also for the populations of the Σ states (Figure 1b), which have populations of a few tenths of percent only, see SI and Figure S6 to S8 for details.

In figure 6a, we show the full time-dependent emission dipole, $\mu(t)$ which is an observable very sensitive to the electronic and vibrational coherences.

$$\mu(t) = \mathrm{Tr}\left[\mu\rho^{mol}(t)\right] = \frac{1}{N_o}\sum_{o=1}^{No}\sum_{g=1}^{Ng}\sum_{i,j}^{Ne} c_{gi}^{o}{}^{*}(t)\, c_{gj}^{o}(t)\,\mu_{gi,gj} \qquad (19)$$

Using Eq.(18), $\mu(t)$ can be written in terms of N_{min} the principal components

$$\mu(t) = \mathrm{Tr}\left[\mu\rho^{mol}(t)\right] = \frac{1}{N_o}\sum_{m=1}^{N\min}\sigma_m^2(t_i)\sum_{g=1}^{Ng}\sum_{i,j}^{Ne} u_{gi}^{m}{}^{*}(t)\, u_{gj}^{m}(t)\,\mu_{gi,gj} \qquad (20)$$

From Eq. (20), one sees that beatings of the emission dipole correspond to electronic coherences between Π states or between excited Σ states since the molecular singulars vectors project electronic states of a given symmetry (see Figure 4 above). The fast ≈ 2 fs periods are the beatings between the Π_1 and the Π_3 states and those between Σ_1 and Σ_2. The longer beatings with a ≈ 10 fs period correspond to the beatings of the electronic coherences between the higher Σ excited states. Note that the amplitudes of the beatings of $\mu(t)$ decrease in time because while the GS and Σ_1 are bound, all the other excited states, including Π_1 are dissociative and the electronic coherences fade away. The revival of the fast period at ≈ 80 fs corresponds to the revival of the $\Sigma_1 - \Sigma_2$ coherence when the wave packet on Σ_1 recurs to the FC region where a small fraction of population is trapped in Σ_2. The relative error on the emission dipole computed for an increasing number of principal components is plotted in Figure 6b. One can see that 5 principal components give a relative error of 10^{-5}-10^{-4}, similar to that computed for the populations of the electronic states while already for 10 components, an error of 10^{-8} is reached. As for the populations, the largest error is made in the first 50 fs when the NAC between the Σ states is strong. Figure 6a shows that the electronic and vibrational

coherences are robust with respect to averaging over random molecular orientations and we come back to this point in the following section.

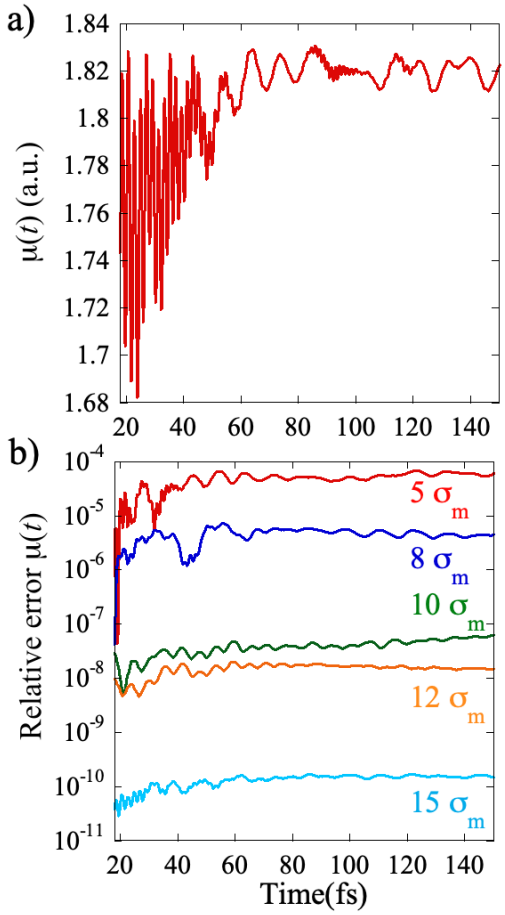

Figure 6. a) Absolute value of the emission dipole moment, $|\mu(t)|$, computed for the exact averaging over 800 random orientation for the exciting 2fs deep UV (4.35 eV) pulse. b) relative error on $\mu(t)$ computed for an increasing number of principal components as indicated.

The results reported in Figures 6b, and S6a and 6b, S7a and 7b and S8 of the SI show that one can accurately describe the dynamics of the ensemble after the pulse is over by solving numerically the TDSE for the 5 molecular singular vectors, $\mathbf{U_m}$, instead of the 800 needed for an averaging over the initial random orientations. This represent a considerable saving of computer time and storage. One only need to propagate and store these 800 random oriented initial vectors during the pulse, for a dozen of femtosecond or so. The accuracy of the SVD propagation can be set by fixing a threshold for the recovery. For a threshold of the order of the accuracy of the numerical integration of the TDSE, one get essentially 'exact' results, as seen already for Figure 6b. Setting a larger threshold inevitably introduces small errors in the populations of the electronic states. Another measure of the error is to use the Frobenius

distance between the 'exact' density matrix obtained from averaging over 800 random initial orientations and the one recovered by propagating a small number of $\mathbf{U_m}$ vectors. The Frobenius distance provides a measure of the error for the entire density matrix, and not only for its diagonal matrix elements as is provided by the difference in the trace, Δ_{Nmin} (Eq.(16)) . The Frobenius distance is plotted in figure S9 on a log scale at t = 18 fs for an increasing number of principal components. Its distance is of the same order of magnitude as Δ_{Nmin} (Eq.(16)) (Figure 3a) and of the error of on time-dependent dipole, $\mu(t)$, (Figure 6a) and decreases in a similar way with increasing the number of principal components included to recover the density matrix.

The expansion in terms of principal components, Eq. (18), is exact when all the N_o principal components are included. Otherwise the SVD theorem[19] states that including more singular values in the expansion will improve the fit or, at worst, not change it. Therefore, in the absence of a benchmark as for the example discussed above, one can readily determine the desired accuracy threshold by increasing the number of singular components used for propagating the TSDE after the pulse, based on the analysis of the magnitude of the singular values and the error on the trace of the ensemble (Figures 3b, S8 and S9) at the end of the pulse, here at 18 fs.

To illustrate further the power of the method, we now discuss the results for a second exciting pulse, with a slightly higher carrier frequency, (5.17 eV) so that the higher Σ and Π states are accessed with similar weights. In this case we only ran the dynamics for the 800 initial random molecular orientations until 18 fs, when the pulse is over. After the pulse is over, the propagation was carried out by integrating the TDSE using a few principal molecular singular vectors, $\mathbf{U_m}$, Eq. ((17)).

We illustrate the convergence process of using an increasing number of principal components for the propagation of the pulse after 18 fs in Figures S10a and S10b (normalized σ_m^2 singular values and errors on the populations) and S9 (Frobenius distance) of the SI. Similarly to the previous example, N_{min}=5 σ_m^2 suffice to converge the SVD description of the ensemble dynamics.

The localization of the $\mathbf{U_m}$ vectors on the grid and on the electronic states at 18 fs is shown in Figure S11. As in the example for the pulse with a lower carrier frequency (Figure 4) $\mathbf{U_1}$ is localized on the GS. For the higher carrier frequency, $\mathbf{U_2}$ is localized on the manifold of excited Σ states, Σ_2, Σ_3 , Σ_4, and $\mathbf{U_3}$ and $\mathbf{U_4}$ on the x and y components of Π_1 and Π_3 respectively.

Correspondingly, the $\mathbf{V_1}$ is uniform, $\mathbf{V_2}$ is localized along z, and $\mathbf{V_3}$ and $\mathbf{V_4}$ are localized along y and x respectively, see Figure S12a-d. Note how for this exciting pulse, σ_2, σ_3 and σ_4 are essentially equal. The small 5th singular component is localized on the excited vibrational states of the GS ($\mathbf{U_5}$) and oriented along *z* ($\mathbf{V_5}$).

The dynamics of the population transfer as well as the total emission dipole, $\mu(t)$, computed by propagating the $\mathbf{U_m}$ vectors, are plotted in Figure 7 for 5 σ_m values and compared to the exact averaging over 800 orientations until 24 fs. We give in figure S13 the differences between the values of the dipole computed for 5 σ_m, 10 σ_m and 15 σ_m. One can see that the value is essentially converged for 5 σ_m. In Figure 7a, one sees a small population transfer between the Π_2 and the Π_3 states which are coupled by NAC at the exit of the FC region while there is extensive population transfer between the states of the Σ manifold. Note how the time dependence of the emission dipole (figure 7b) is different from that shown on Figure 6a for a 2fs pulse with a different carrier frequency. The fast oscillations with a period of ≈ 2 fs are those of the electronic coherences between Π_1 and the Π_3 states (quasi degenerate with the Π_2 in the FC region). However here, they are modulated by the the slower ones (≈ 10fs) which correspond to the electronic coherences between the excited Σ manifold.

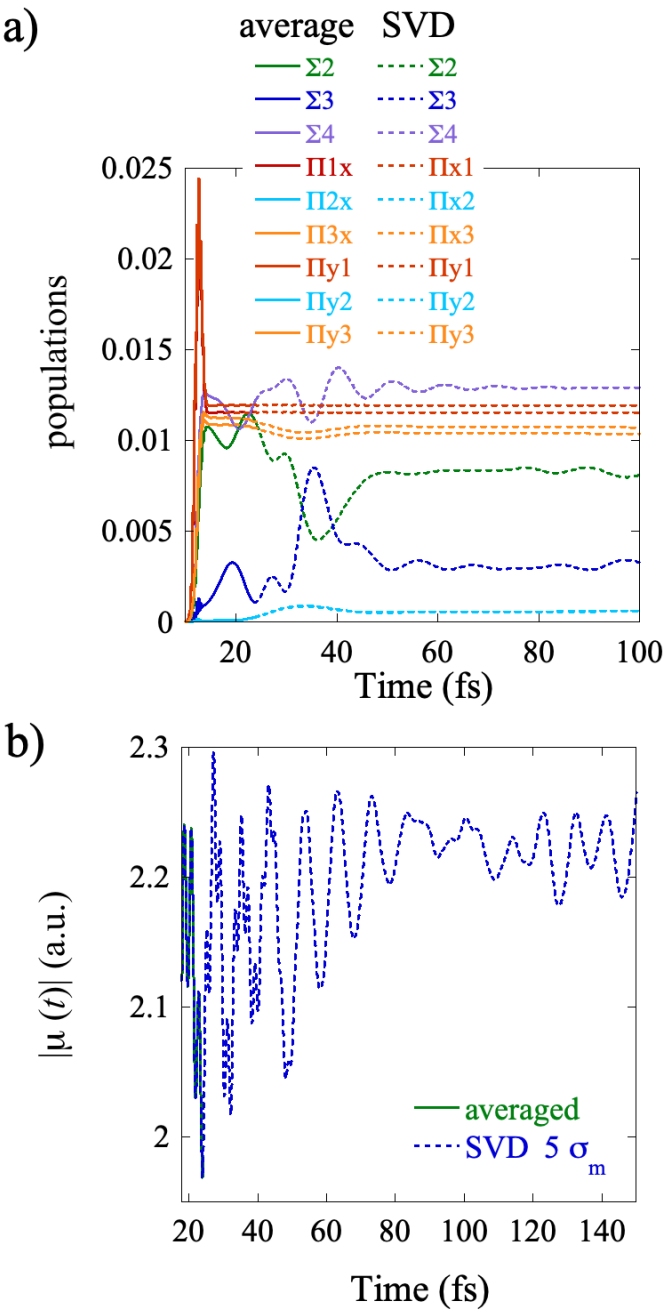

Figure 7. Populations (a) and emission dipole, $|\mu(t)|$, Eq. (20), (b), computed for the excitation by the 2fs deep UV 5.17 eV pulse. In panel a), the exact averaging over 800 initial random orientations is plotted in full lines up to 24fs. For later times, the approximate values computed by the propagation of 5 $\mathbf{U_m}$ vectors using the TDSE (Eq.(17)) is shown in dotted lines, starting at 18 fs. In panel b) the same is done for the full time-dependent dipole, $|\mu(t)|$.

Dynamics of the vibrational and electronic coherences of the ensemble

Figures 6a and 7b show that the total emission dipole $\mu(t)$ averaged over an ensemble of molecular orientations is oscillating with the periods of the electronic and vibrational coherences. However, not all types of electronic coherences survive the orientation averaging. Eqs. (7) and (9) show that only the electronic coherences between electronic states that contribute to the same molecular singular vector, $\mathbf{U_m}$, survive the orientation averaging. This means that there will not be electronic coherences between Σ and Π states in an ensemble of randomly oriented molecules, unlike when a superposition of Σ and Π states is built by exciting oriented LiH molecules with a pulse that has a polarization direction in the (x,z) and in the (x,y) plane of the molecular frame,[5, 26] see figure S14a-c. In the ensemble of randomly oriented molecules, the $\Sigma-\Pi$ coherences average out: only the $\Pi-\Pi$ and $\Sigma-\Sigma$ electronic coherences are present. They are plotted in figure 8a and b respectively for the dynamics induced by the low 4.35 eV frequency 2fs exciting pulse (see figures 1, 4, 5 and 6 above) and in figures 8c and d for the higher frequency one (see figure 7 and figures S11 and S12 of the SI). There is a rich dynamics of the $\Sigma-\Sigma$ coherences that is modulated by the NAC coupling, with electronic coherences between specific electronic states dominating the dynamics at different time ranges. The $\Pi-\Pi$ coherences are much more regular since there is only a weak NAC coupling between the Π_3 and the Π_2 states. The $\Pi_3-\Pi_2$ NAC leads to a small population transfer to Π_2 in the 20-50 fs time range and a Π_2 - Π_1 electronic coherence which does not vanish because the wave packets are moving on very similar dissociative potentials. The $\Pi_3-\Pi_1$ vanishes at around 50 fs because Π_3 is bound (see Figure S1) but Π_1 is dissociative. A slow beating Π_3 - Π_2 electronic coherence is clearly visible in Figure 8c which also vanishes because Π_1 is dissociative. The $\Sigma-\Sigma$ and $\Pi-\Pi$ electronic coherences govern the emission dipole (Eq. (20)) which does not exhibit periods corresponding to $\Sigma-\Pi$ coherences after the pulse, see Figure 6a and Figure 7b.

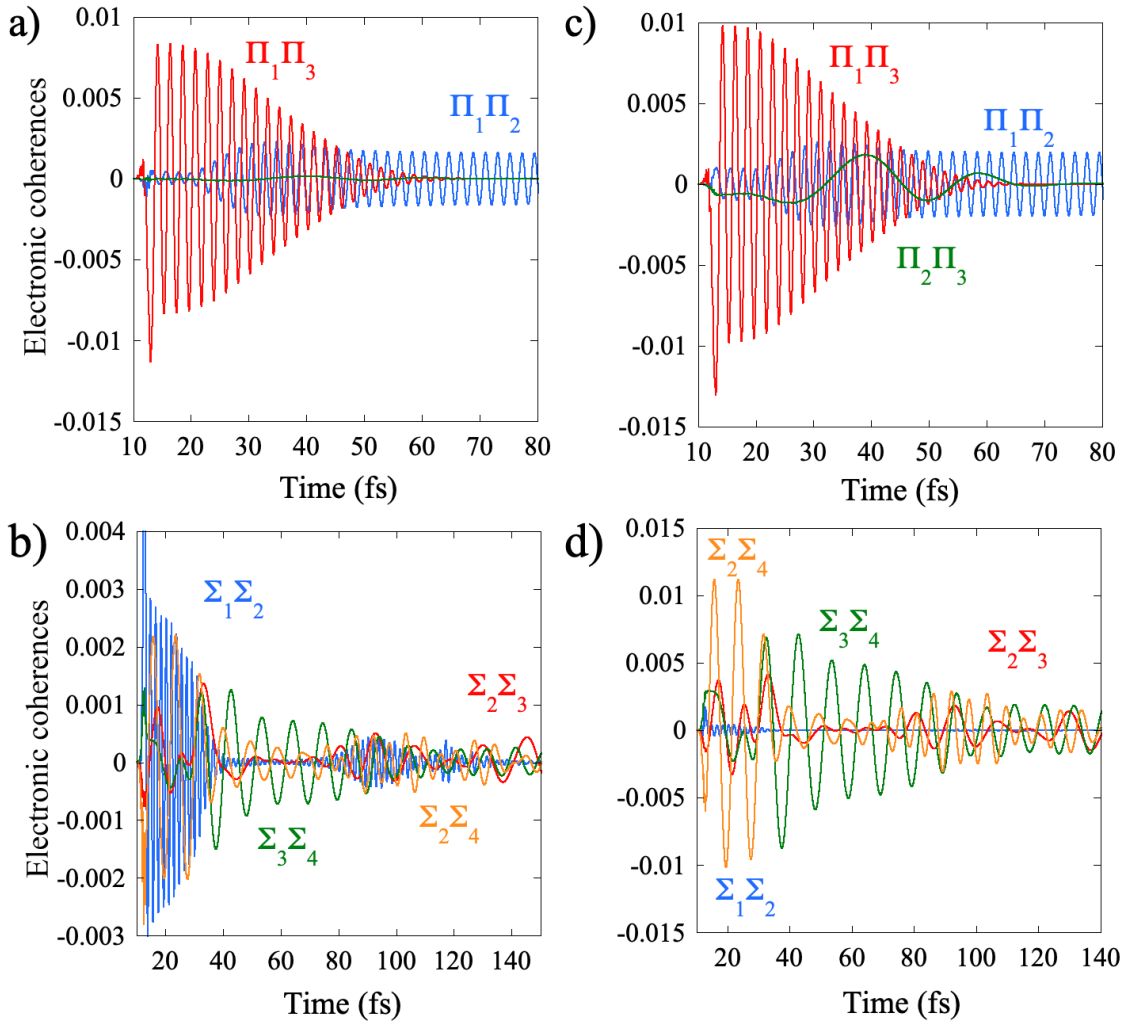

Figure 8: Time-dependence of the electronic coherences for the ensemble of randomly oriented molecules. a) and b) : dynamics induced by the lower frequency 4.35 eV exciting pulse. c) and d) dynamics induced by the higher frequency 5.17 eV exciting pulse.

Vibrational coherences are also robust with respect to molecular averaging as can be seen from Figure 9a-h, where plots of heatmaps of the reduced nuclear density matrix, $\rho_{nuc,m}^{mol}(t)$, Eq. (8) , that correspond to the largest three principal components, m=1, 2, 3, are shown for the lower frequency, 4.35 eV, exciting pulse. Two times are shown, the time t=18fs, at which the SVD analysis is carried out after the pulse and t = 50fs at the end of the region of strong NAC interactions between the Σ states (see Figure 1b for the population dynamics and Figure 4 for the localization of the largest principal components), which induces more complex patterns in

the heatmap (figure 9f) of the third principal components localized on Σ states than on the second principal component localized on Π states, see figure 4 above.

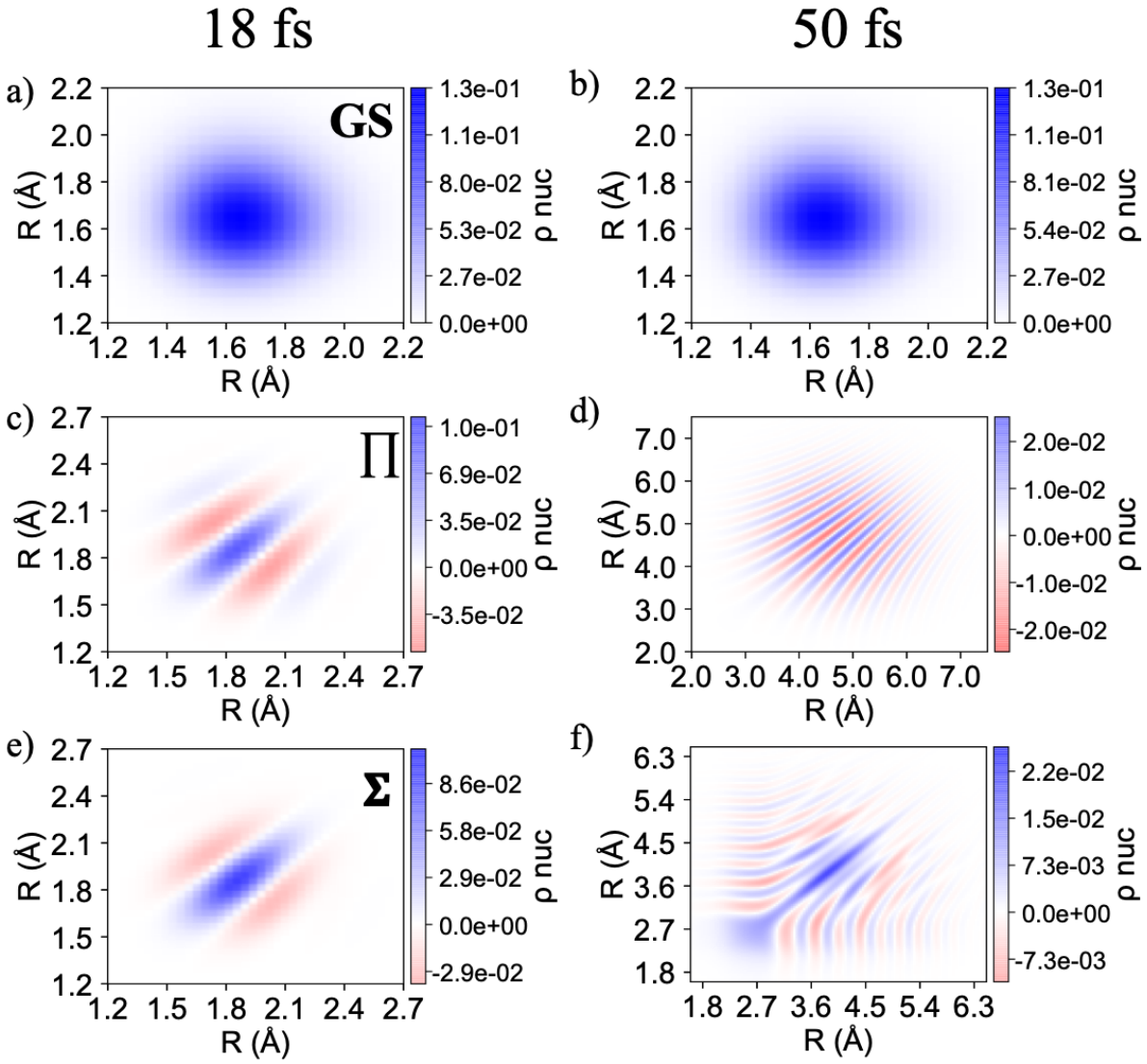

Figure 9. Heat maps of the real part of the reduced nuclear density, $\rho^{mol}_{nuc,m}(t)$ m= 1,2,3, Eq.(8), computed at 18fs (left column) and 50 fs (right column) for the lower carrier frequency (4.35 eV) exciting pulse. a) and b): Largest principal component, m=1, that is localized on the GS. c) and d): second largest, m=2, localized on the Π_1 state. e) and f) third largest, m=3, localized on the Σ states (see figure 4)

The same overall behavior is recovered for the higher frequency exciting 2fs pulse, see Figure S15a-j. The difference is that one can identify the effect of the $\Pi_3 - \Pi_2$ NAC coupling in the hestmap of the $\rho^{mol}_{nuc,m}(t)$ for the third principal component.

Conclusions

Our SVD based method allows for accurately describing the dynamics of the coherent excitation of an ensemble of randomly oriented molecules by a broad in energy ultrashort pulse that encompasses several electronic states. It shows that rather few singular vectors are sufficient to represent the ensemble of orientations of attosecond excited molecules. For excitations by the reasonably strong 2fs pulses used in the numerical examples ($3.51\ 10^{12}$ W/cm^2) the number of singular orientations is nevertheless larger than the 3 cartesian orientations expected in the linear regime. Equally noteworthy is that fewer than expected singular vectors are sufficient to represent the ensemble of excited electronic states. Even beyond that, note the stereodynamics: there is a one to one correspondence between the two sets of singular vectors. Each dominant orientation is thereby associated with its own coherent set of excited electronic states. Our derivation and numerical examples show that electronic coherences within the coherent state associated with a specific molecular orientation of the ensemble are robust with respect to orientation averaging while those between electronic states belonging to coherent states that correspond to different principal orientations are washed out by the orientation averaging. From a numerical point of view, the SVD provides a storage and computer time efficient approach for studying the dynamics of coherently excited randomly oriented molecules. Future work will address multiphoton photoexcitation by stronger (with peak intensity in the range 10^{13}-10^{14} W/cm^2) few cycle NIR pulses as well as the excitation of non linear molecules for which it is expected that a few additional principal orientations will be required for describing the dynamics of ensemble of initially randomly oriented molecules.

Supporting information. Supplemental figures and a detailed derivation of the SVD approach for a sudden photoexcitation process.

Acknowledgments

FR and MCG acknowledge the support of the Fonds National de la Recherche (F.R.S.-FNRS, Belgium), #T0205.20, and of the action of concerted research MECHANOCHEM (ARC 19/23-20, ULiege). Computational resources have been provided by the Consortium des Equipements de Calcul Intensif (CECI), funded by the F.R.S.-FNRS under Grant # 2.5020.11 The authors thanks the COST action ATTOCHEM (CA18222).

References

1. Vrakking, M. J. J.; Lepine, F., *Attosecond Molecular Dynamics*. The Royal Society of Chemistry: Cambridge, 2019; p P001-500.
2. Nisoli, M.; Decleva, P.; Calegari, F.; Palacios, A.; Martín, F., Attosecond Electron Dynamics in Molecules. *Chem. Rev.* **2017**, *117*, 10760-10825.
3. Merritt, I. C. D.; Jacquemin, D.; Vacher, M., Attochemistry: Is Controlling Electrons the Future of Photochemistry? *J. Phys. Chem. Lett.* **2021**, *12*, 8404-8415.
4. Remacle, F.; Levine, R. D., An Electronic Time Scale for Chemistry. *Proc. Natl. Acad. Sci. USA* **2006**, *103*, 6793-6798.
5. Remacle, F.; Nest, M.; Levine, R. D., Laser Steered Ultrafast Quantum Dynamics of Electrons in Lih. *Phys. Rev. Lett.* **2007**, *99*, 183902.
6. Stapelfeldt, H.; Seideman, T., Colloquium: Aligning Molecules with Strong Laser Pulses. *Rev. Mod. Phys.* **2003**, *75*, 543-557.
7. Gordon, R. J.; Zhu, L.; Seideman, T., Coherent Control of Chemical Reactions. *Acc. Chem. Res.* **1999**, *32*, 1007-1016.
8. Ghafur, O.; Rouzee, A.; Gijsbertsen, A.; Siu, W. K.; Stolte, S.; Vrakking, M. J. J., Impulsive Orientation and Alignment of Quantum-State-Selected No Molecules. *Nature Physics* **2009**, *5*, 289-293.
9. Kraus, P. M.; Baykusheva, D.; Wörner, H. J., Two-Pulse Field-Free Orientation Reveals Anisotropy of Molecular Shape Resonance. *Phys. Rev. Lett.* **2014**, *113*, 023001.
10. Fleischer, S.; Zhou, Y.; Field, R. W.; Nelson, K. A., Molecular Orientation and Alignment by Intense Single-Cycle Thz Pulses. *Phys. Rev. Lett.* **2011**, *107*, 163603.
11. Zare, R. N., *Angular Momentum, Understanding Spatial Aspects in Chemistry and Physics*; Wiley: New York, 1991.
12. Bernstein, R. B., *Chemical Dynamics Via Molecular Beam and Laser Techniques*; Oxford University Press: Oxford, 1992.
13. Bernstein, R. B.; Herschbach, D. R.; Levine, R. D., Dynamical Aspects of Stereochemistry. *J. Phys. Chem.* **1987**, *91*, 5365-5377.
14. Calegari, F., et al., Ultrafast Electron Dynamics in Phenylalanine Initiated by Attosecond Pulses. *Science* **2014**, *346*, 336-339.
15. Kraus, P. M., et al., Measurement and Laser Control of Attosecond Charge Migration in Ionized Iodoacetylene. *Science* **2015**, *350*, 790-795.
16. Valentini, A.; van den Wildenberg, S.; Remacle, F., Selective Bond Formation Triggered by Short Optical Pulses: Quantum Dynamics of a Four-Center Ring Closure. *Phys. Chem. Chem. Phys.* **2020**, *22*, 22302-22313.
17. Månsson, E. P., et al., Real-Time Observation of a Correlation-Driven Sub 3 Fs Charge Migration in Ionised Adenine. *Commun. Chem.* **2021**, *4*, 73.
18. Schwickert, D., et al., Electronic Quantum Coherence in Glycine Molecules Probed with Ultrashort X-Ray Pulses in Real Time. *Sci. Adv.* **2022**, *8*, eabn6848.
19. Golub, G. H.; Reinsch, C., Singular Value Decomposition and Least Squares Solutions. In *Linear Algebra*, Wilkinson, J. H.; Reinsch, C.; Bauer, F. L., Eds. Springer Berlin Heidelberg: Berlin, Heidelberg, 1971; pp 134-151.
20. Jaynes, E. T., Information Theory and Statistical Mechanics. Ii. *Phys. Rev.* **1957**, *108*, 171-190.
21. Gonçalves, C. E. M.; Levine, R. D.; Remacle, F., Ultrafast Geometrical Reorganization of a Methane Cation Upon Sudden Ionization: An Isotope Effect on Electronic Non-Equilibrium Quantum Dynamics. *Phys. Chem. Chem. Phys.* **2021**, *23*, 12051-12059.
22. Galli, M., et al., Generation of Deep Ultraviolet Sub-2-Fs Pulses. *Opt. Lett.* **2019**, *44*, 1308-1311.
23. Wanie, V., et al., Ultraviolet Supercontinuum Generation Using a Differentially-Pumped Integrated Glass Chip. *Journal of Physics: Photonics* **2024**, *6*, 025005.

24. Brahms, C.; Travers, J. C., Efficient and Compact Source of Tuneable Ultrafast Deep Ultraviolet Laser Pulses at 50 Khz Repetition Rate. *Opt. Lett.* **2023**, *48*, 151-154.
25. van den Wildenberg, S.; Mignolet, B.; Levine, R. D.; Remacle, F., Temporal and Spatially Resolved Imaging of the Correlated Nuclear-Electronic Dynamics and of the Ionized Photoelectron in a Coherently Electronically Highly Excited Vibrating Lih Molecule. *J. Chem. Phys.* **2019**, *151*, 134310.
26. Nikodem, A.; Levine, R. D.; Remacle, F., Spatial and Temporal Control of Populations, Branching Ratios, and Electronic Coherences in Lih by a Single One-Cycle Infrared Pulse. *Phys. Rev. A* **2017**, *95*, 053404.

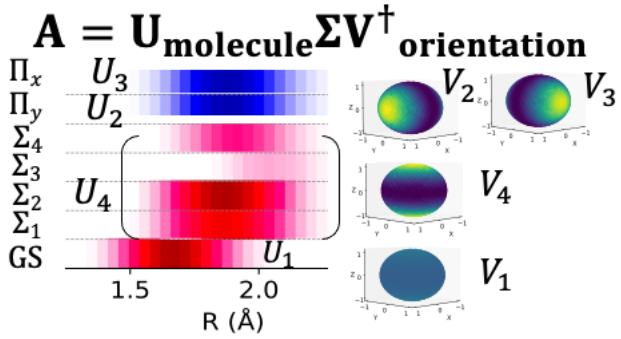

TOC